SUPPLEMENTARY

# NEURAL-NETWORK DEEP POTENTIAL MODELS FOR LITHIUM ADSORPTION ON C–N–O-MODIFIED CARBON MATERIALS

*Sergey A. Sozykin, Valery P. Beskachko*

South Ural State University, 454080 Chelyabinsk

sozykinsa@susu.ru

## Dataset composition

The table S1 summarises the different system types included in the dataset, along with a representative atomic structure for each type and the number of corresponding configurations. For equilibrium structures, the simulation cell parameters are also provided.

**Table S1. Composition of the reference dataset**

| System type, cell parameters (for stable models) | Structure | Number of structures in dataset |
|---|---|---|
| graphene, a=17.27, b=17.27 | 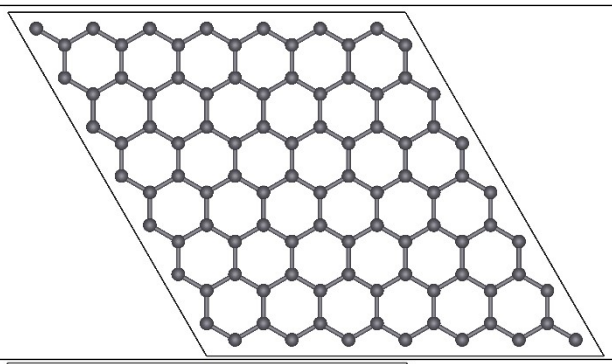 | 282 |
| graphene_vac – graphene with vacancy defect | 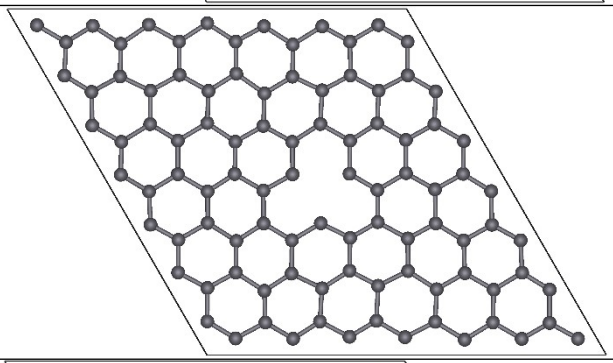 | 89 |
| graphene_dvac – graphene with double vacancy defect | 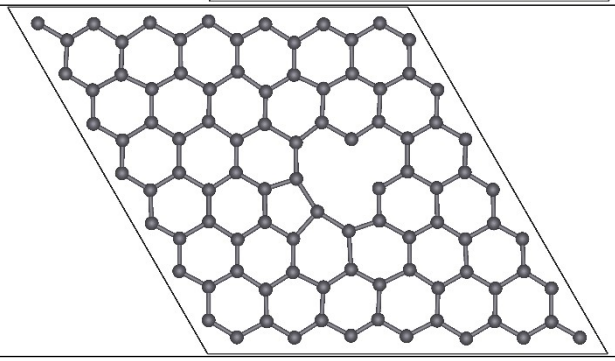 | 61 |

| | | |
|---|---|---|
| graphite | 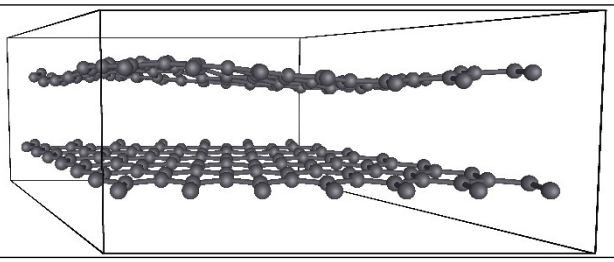 | 480 |
| SWNT(5,5) – single-walled carbon nanotube (5,5), c=12.33 | 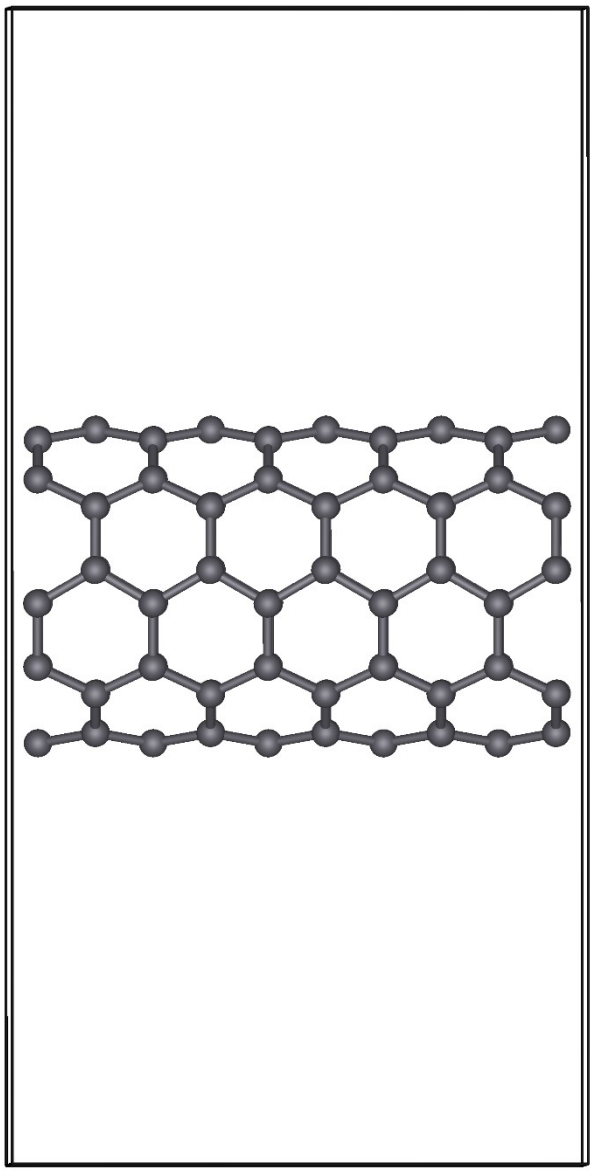 | 1339 |

| | | |
|---|---|---|
| SWNT(8,0) – single-walled carbon nanotube (8,0), c=17.04 | 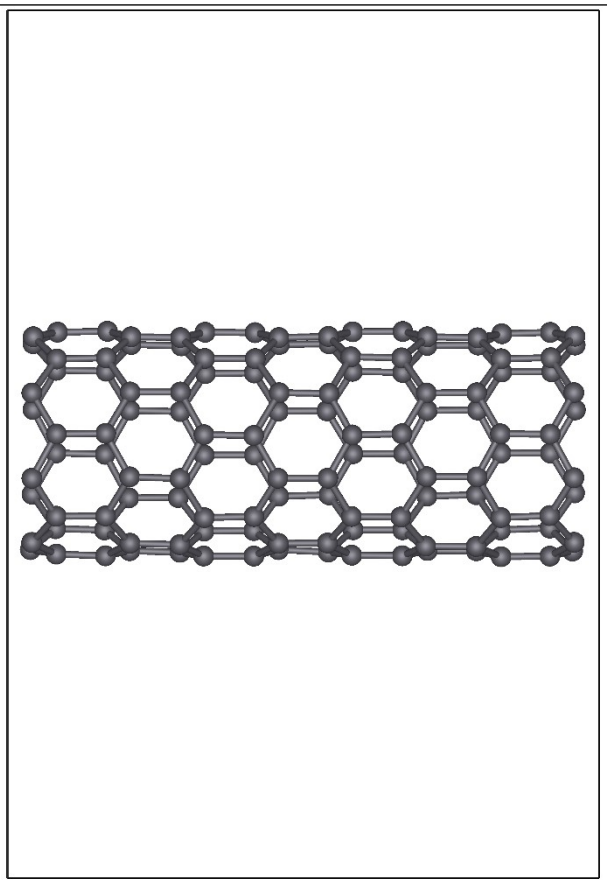 | 1609 |
| biphenylene, 18.08 15.05 25.11 | 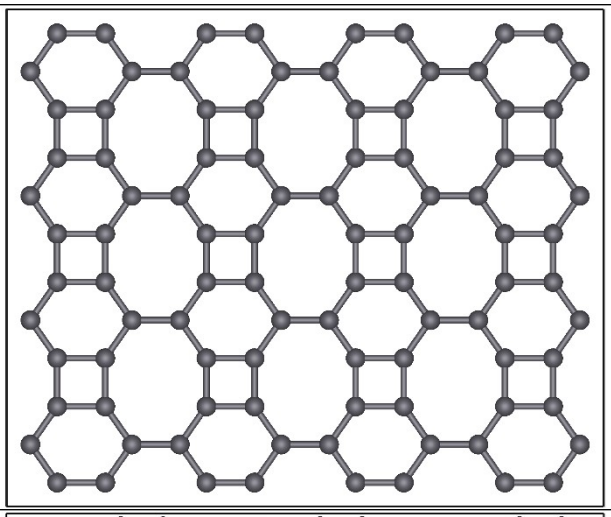 | 139 |
| psi-graphene, a=20.12, b=14.51 | 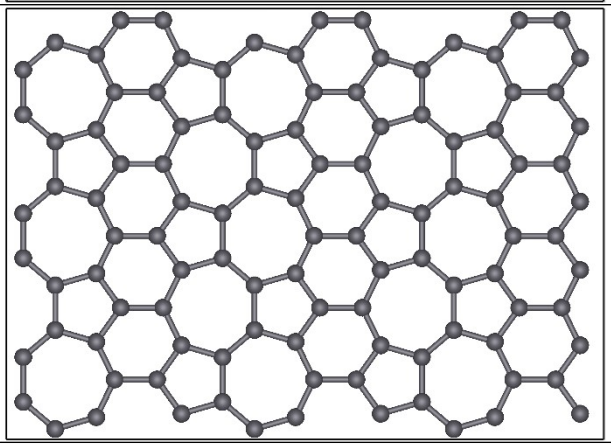 | 171 |

| | | |
|---|---|---|
| irida-graphene,<br>a=18.95, b=18.95 | 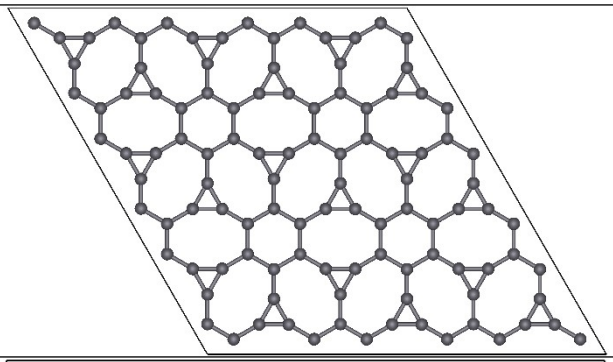 | 161 |
| tpdh-graphene,<br>a=19.77, b=13.94 | 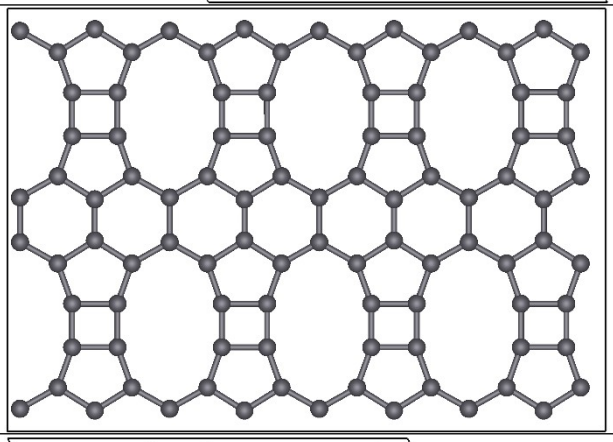 | 110 |
| N-graphene – graphene with a substitutional nitrogen defect | 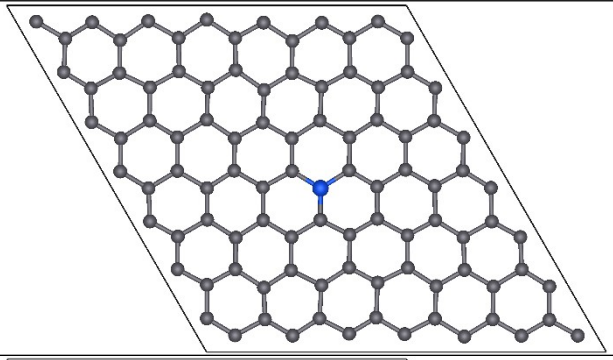 | 387 |
| N-pyridinic – graphene containing pyridinic nitrogen | 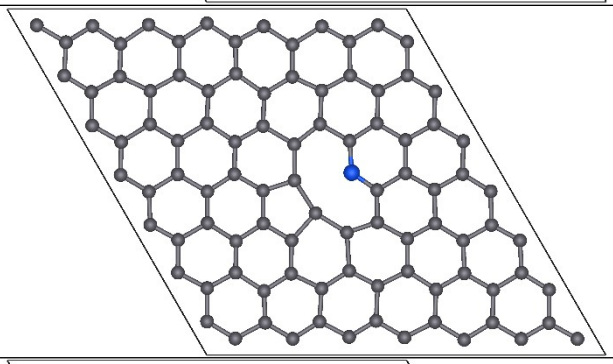 | 433 |
| $C_2N$,<br>a=16.65, b=16.65 | 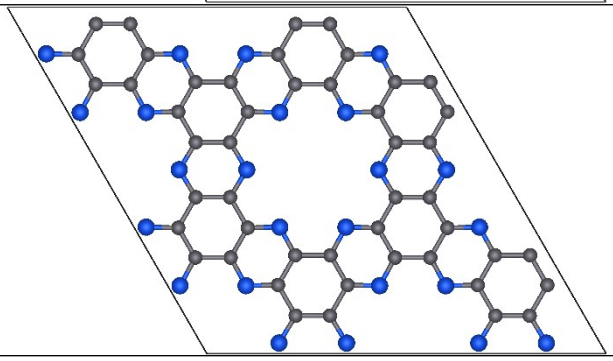 | 2159 |

| | | |
|---|---|---|
| $C_2N$_3D – stacked $C_2N$ structure with three-dimensional periodicity | 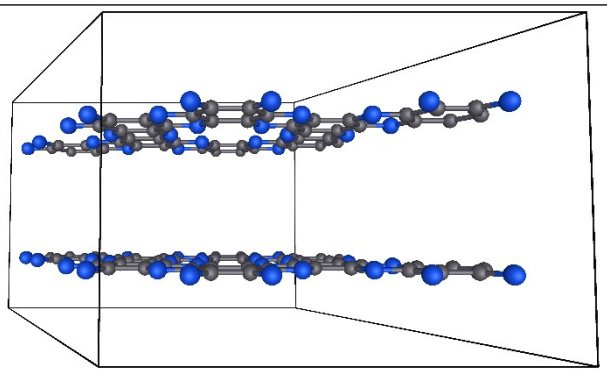 | 337 |
| C2N+3Li – $C_2N$ with three adsorbed Li atoms | 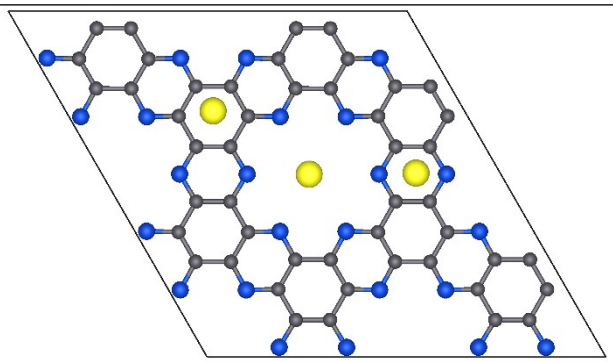 | 1566 |
| C2N_3D+3Li – stacked $C_2N$ structure with three-dimensional periodicity and three adsorbed Li atoms per $C_2N$ layer | 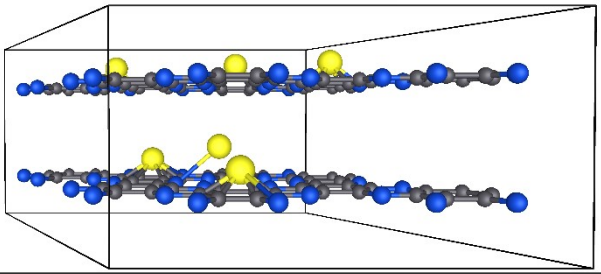 | 48 |
| graphene+1Li – graphene with one adsorbed Li atom, a=17.28, b=17.28 | 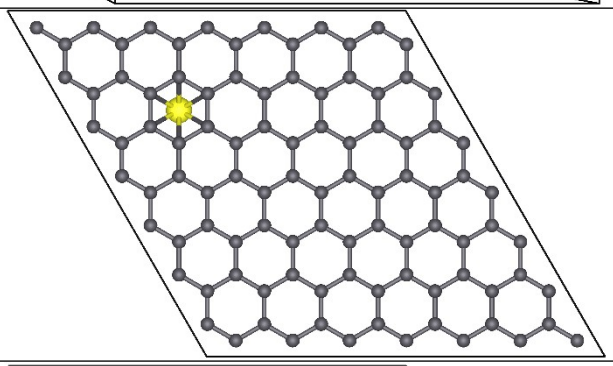 | 271 |
| graphene+3Li – graphene with three adsorbed Li atoms | 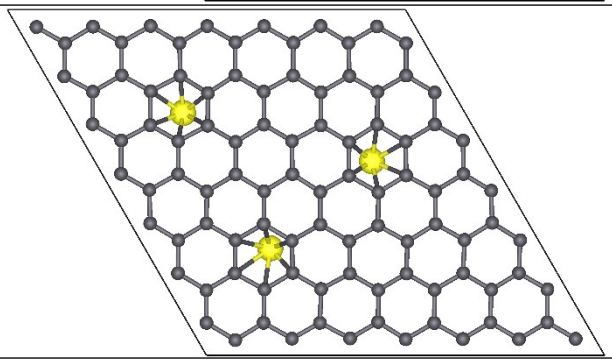 | 292 |

| | | |
|---|---|---|
| graphite+3Li – graphite with three adsorbed Li atoms per graphene layer | 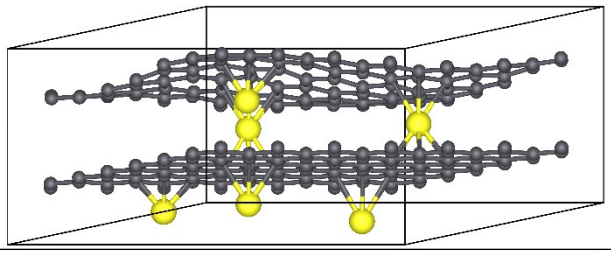 | 675 |
| biphenylene+3Li – biphenylene with three adsorbed Li atoms | 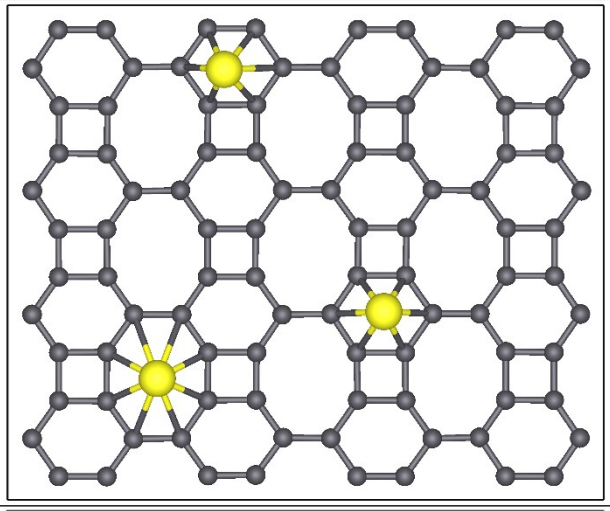 | 389 |
| psi-graphene+3Li – psi-graphene with three adsorbed Li atoms | 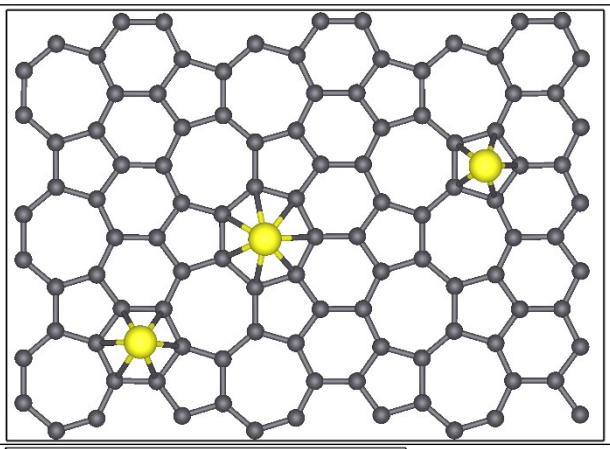 | 423 |
| irida-graphene+3Li – irida-graphene with three adsorbed Li atoms | 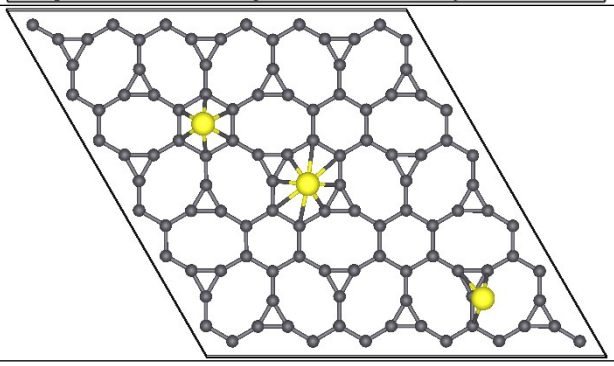 | 570 |

| | | |
|---|---|---|
| tpdh-graphene+4Li – tpdh-graphene with four adsorbed Li atoms | 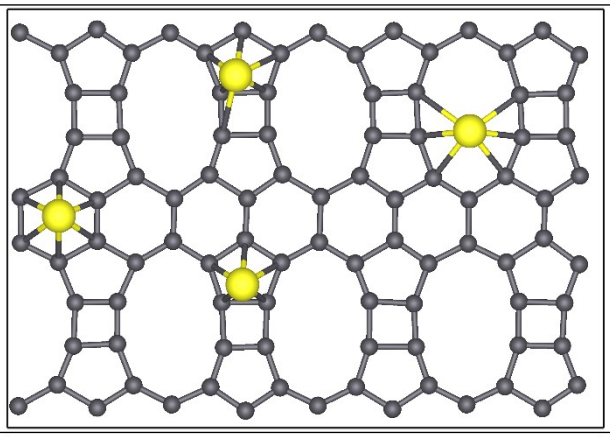 | 435 |
| SWNT(5, 5)+1Li – SWNT(5, 5) with one adsorbed Li atom | 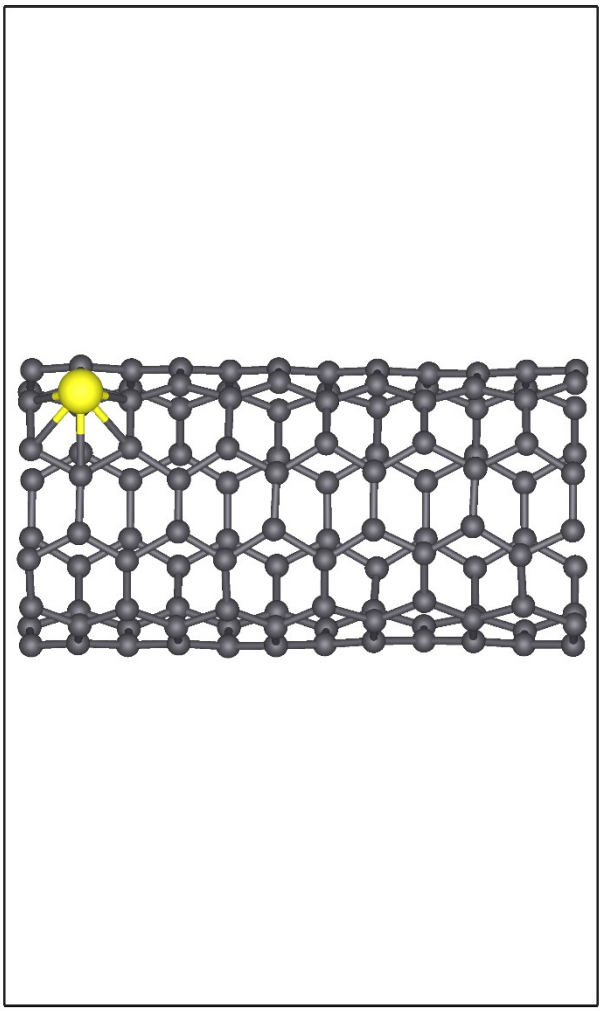 | 658 |

| | | |
|---|---|---|
| SWNT(5, 5)+5Li – SWNT(5, 5) with five adsorbed Li atoms | 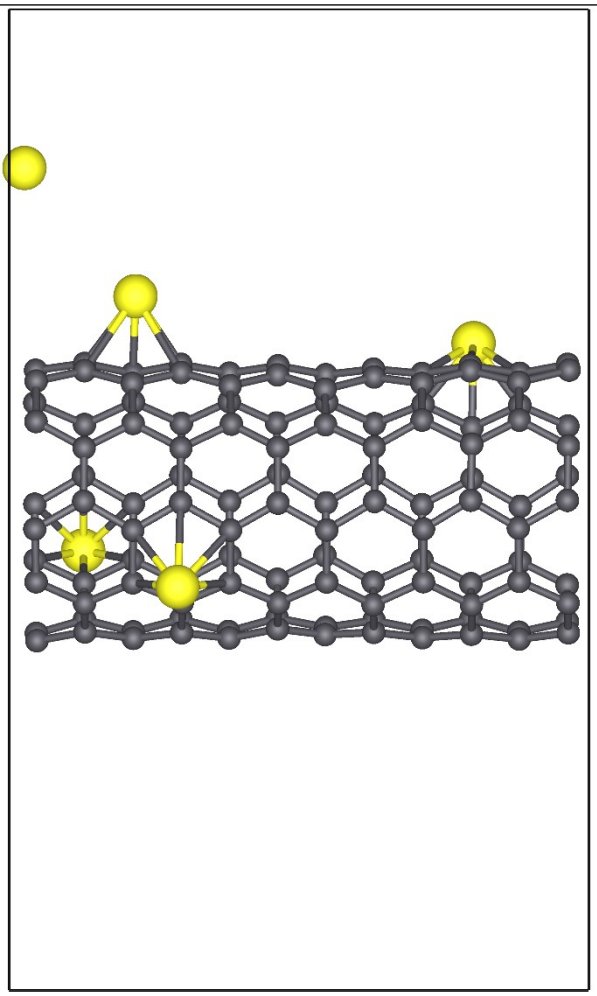 | 260 |

| | | |
|---|---|---|
| SWNT(5, 5)+10Li – SWNT(5, 5) with ten adsorbed Li atoms | 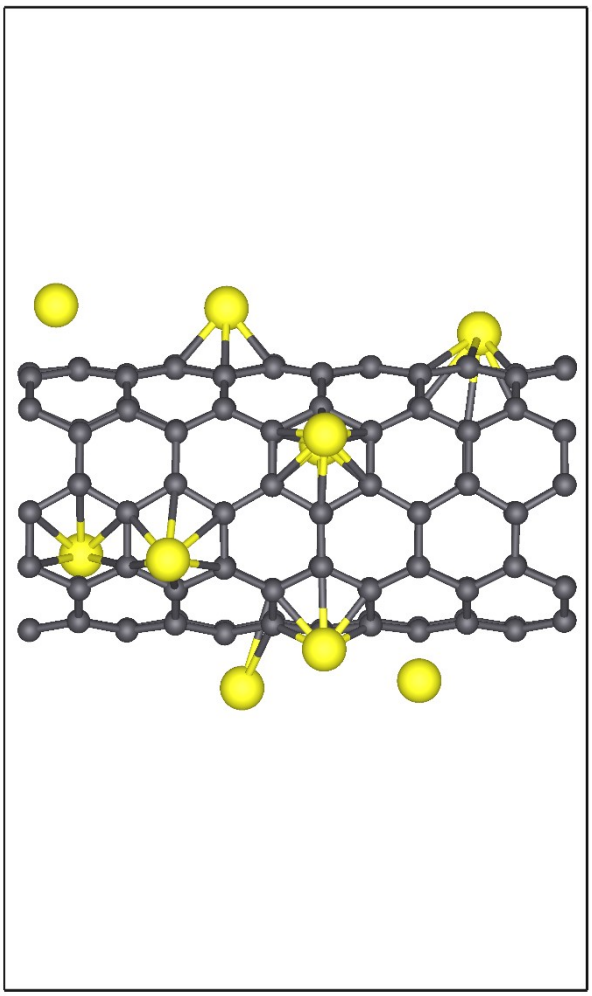 | 232 |
| SWNT(8, 0)+5Li – SWNT(8, 0) with five adsorbed Li atoms | 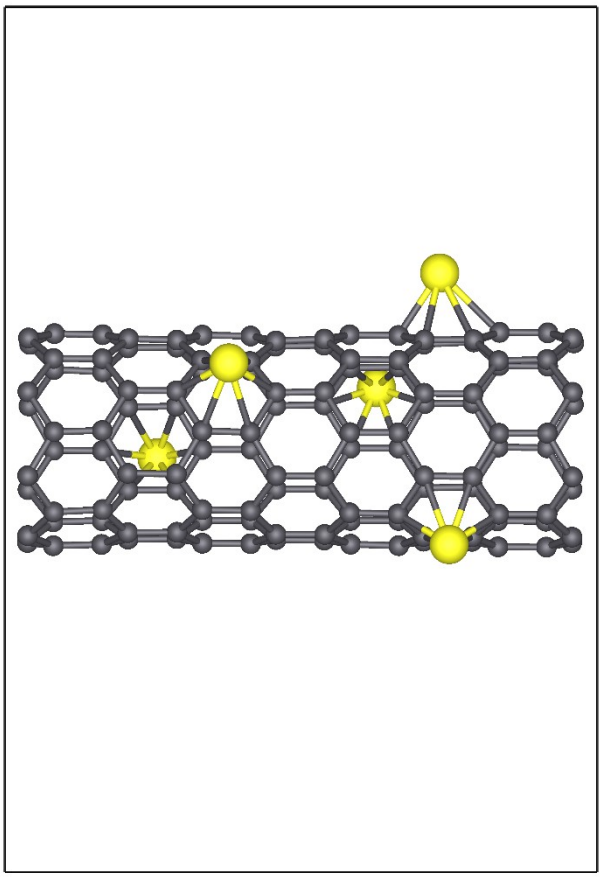 | 88 |

| | | |
|---|---|---|
| SWNT(8, 0)+10Li – SWNT(8, 0) with ten adsorbed Li atoms | 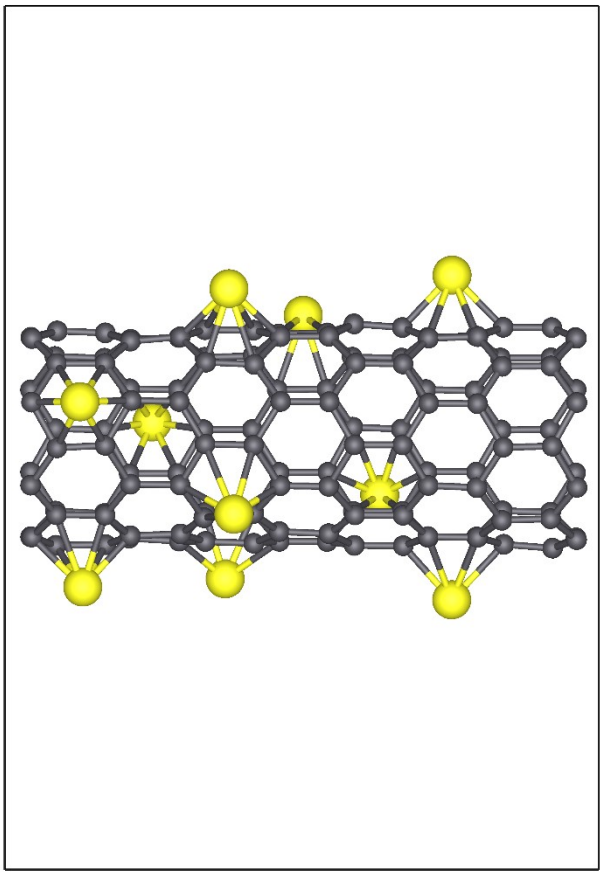 | 47 |
| TOC | 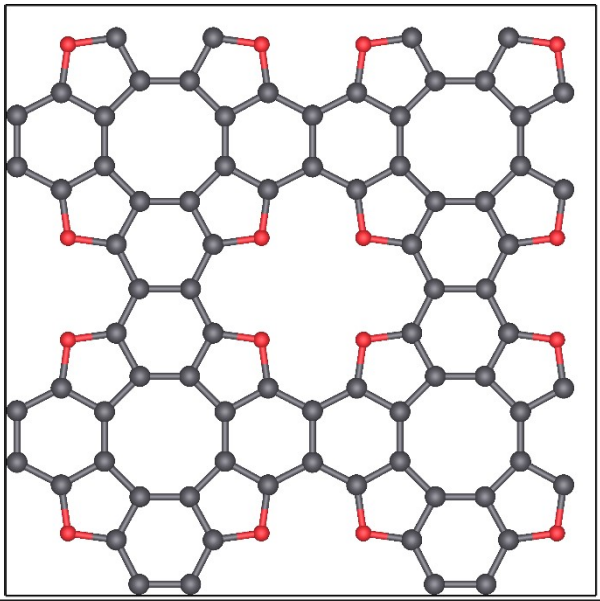 | 1923 |
| TOC_3D – stacked TOC structure with three-dimensional periodicity | 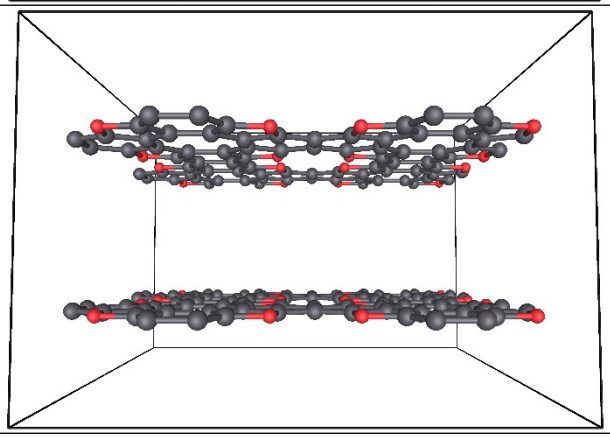 | 479 |

| | | |
|---|---|---|
| TOC+3Li – TOC with three adsorbed Li atoms | 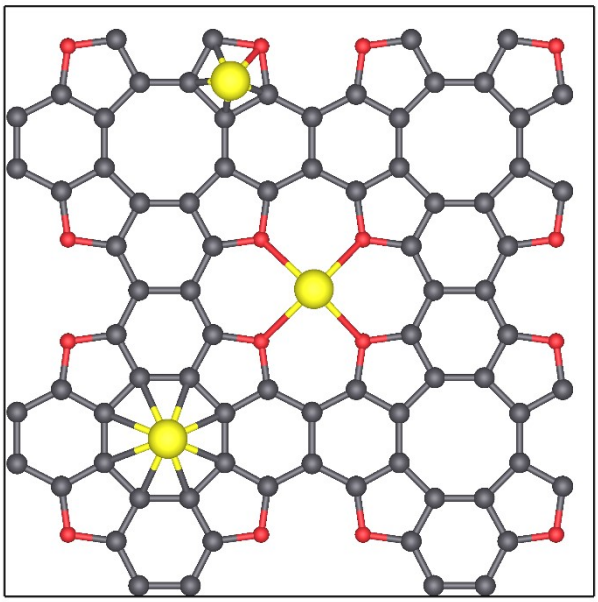 | 951 |
| TOC_3D+3Li – stacked TOC structure with three-dimensional periodicity and three adsorbed 3 Li atoms per TOC layer) | 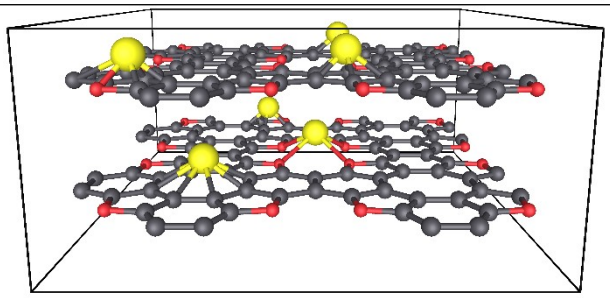 | 84 |
| $Li_2$ – dimer | 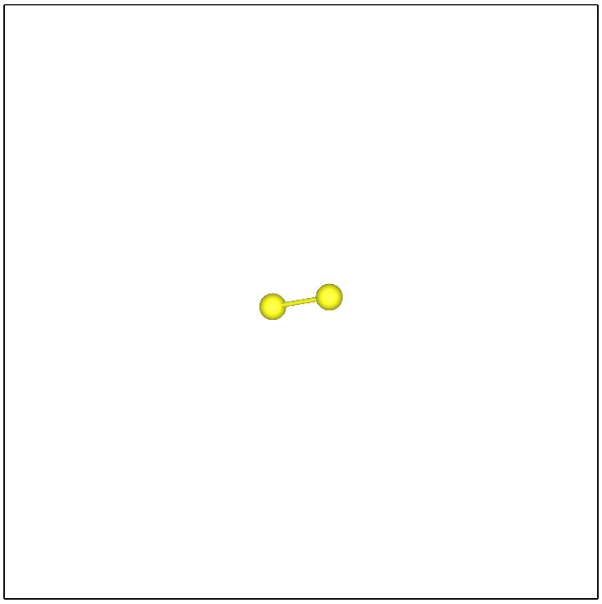 | 153 |

| | | |
|---|---|---|
| $Li_3$ – trimer | 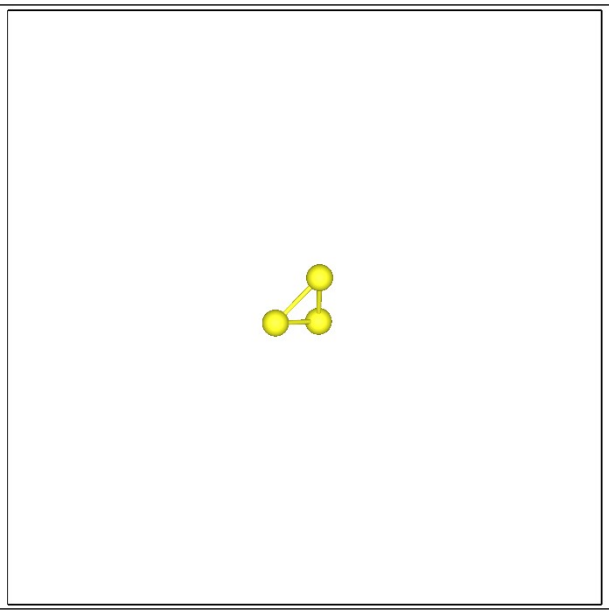 | 140 |

Table S2 summarises the external test systems that were not included in the training dataset, together with representative atomic structures and the corresponding simulation cell parameters.

**Table S2. Test systems not included in the training dataset**

| System type | Structure |
|---|---|
| SWNT(6,2) – single-walled carbon nanotube (6,2), c=15.41 | 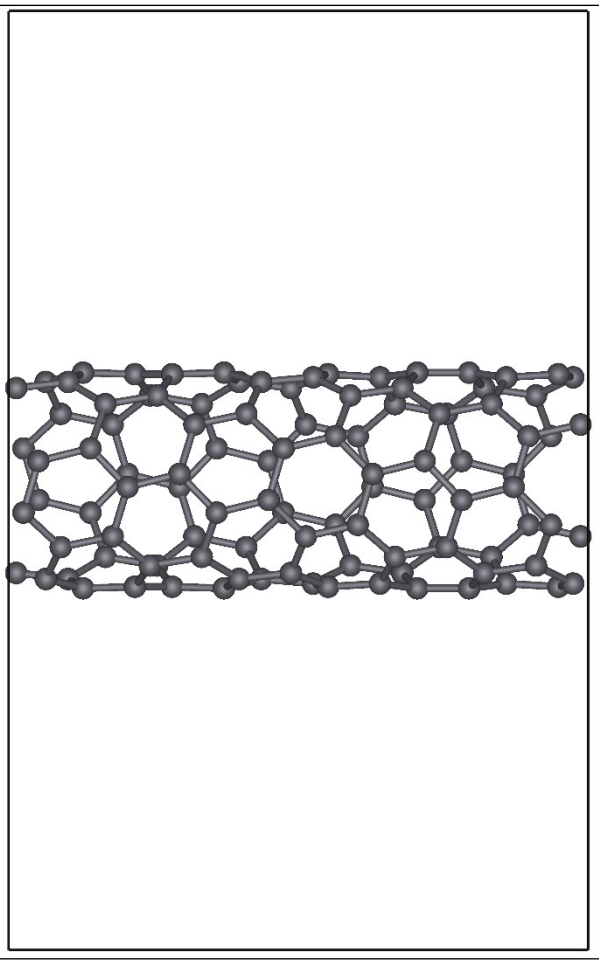 |

| | | | |
|---|---|---|---|
| SWNT(7,3) – single-walled carbon nanotube (7,3), c=13.74 | | 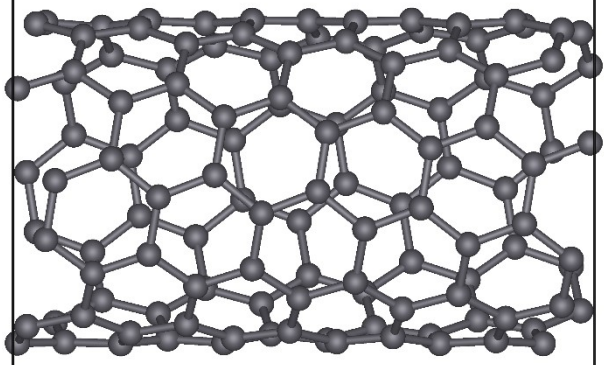 | |

| | |
|---|---|
| SWNT(7,7) – single-walled carbon nanotube (7,7), c=14.80 | 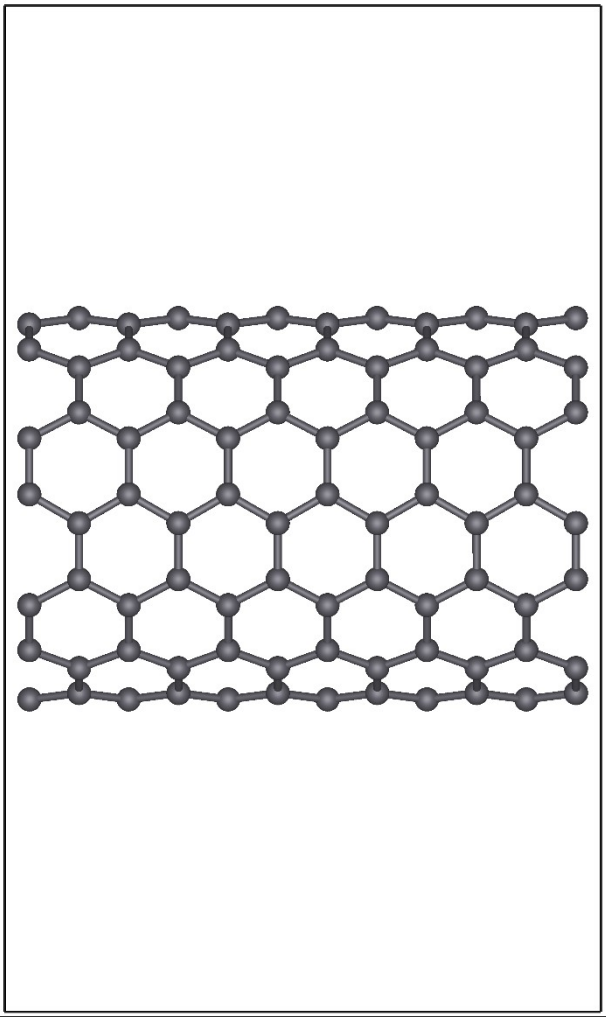 |

| | |
|---|---|
| SWNT(8,8) – single-walled carbon nanotube (8,8), c=14.80 | 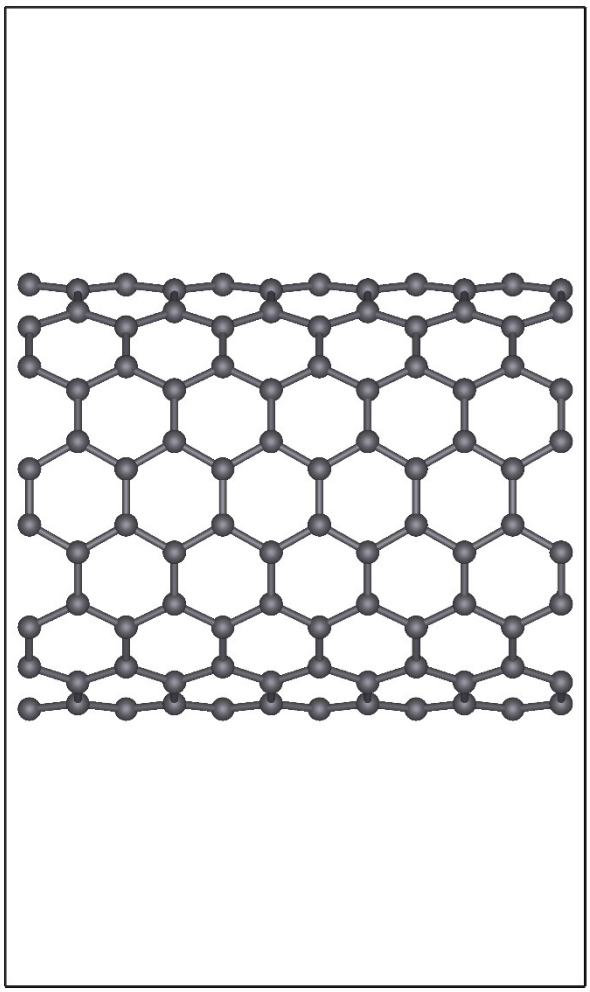 |
| SWNT(9,0) – single-walled carbon nanotube (9,0), c=17.10 | 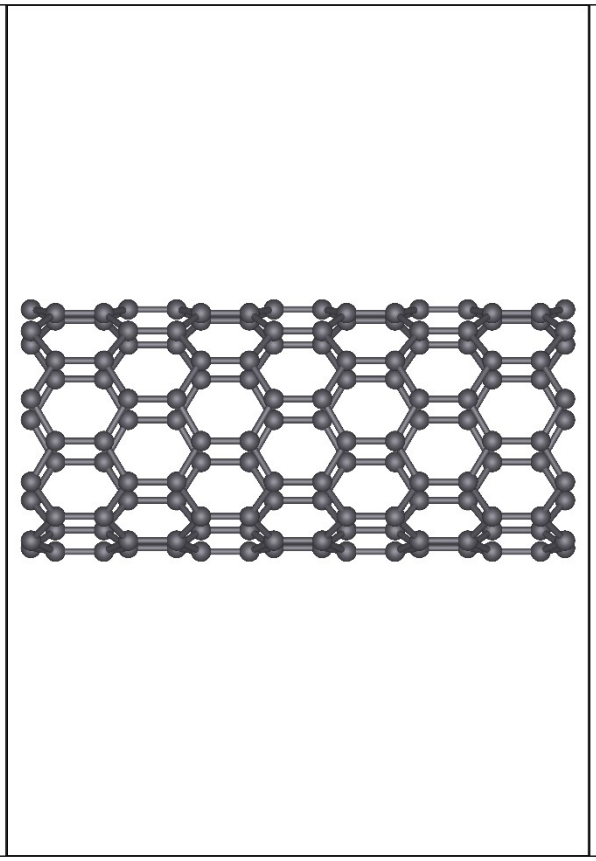 |

| | |
|---|---|
| SWNT(10,0) – single-walled carbon nanotube (10,0), c=17.11 | 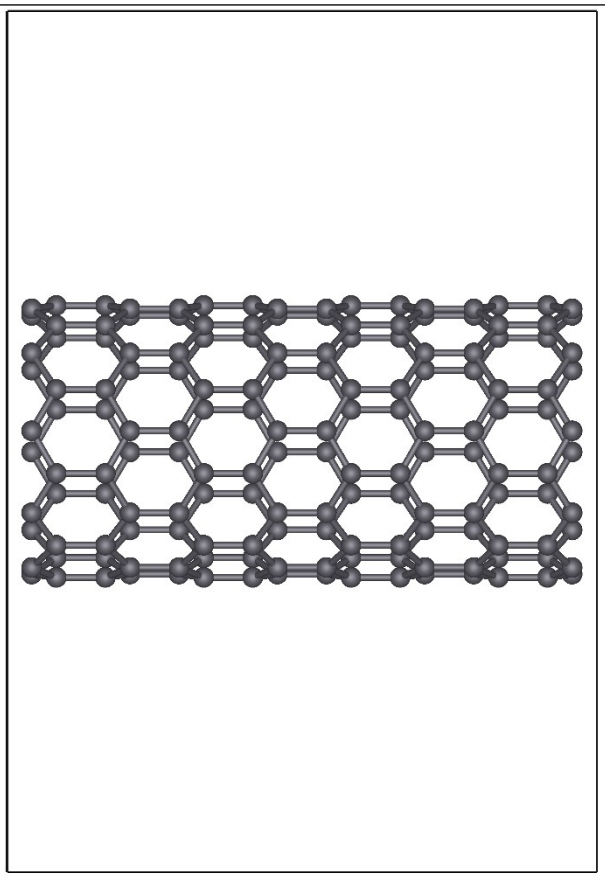 |

**RMSE of energies and force magnitudes**

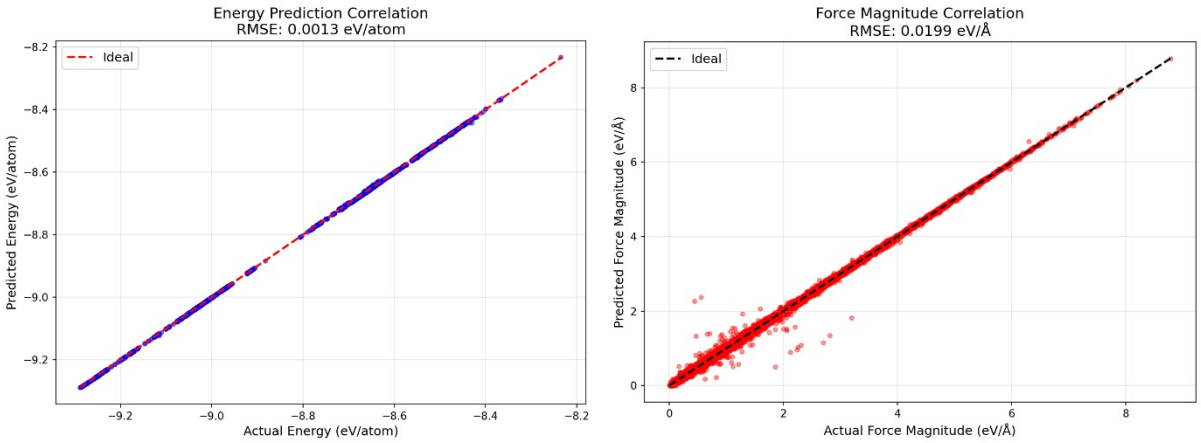


Figure S1. RMSE of energies and force magnitudes for DPA-3.1-fine potential

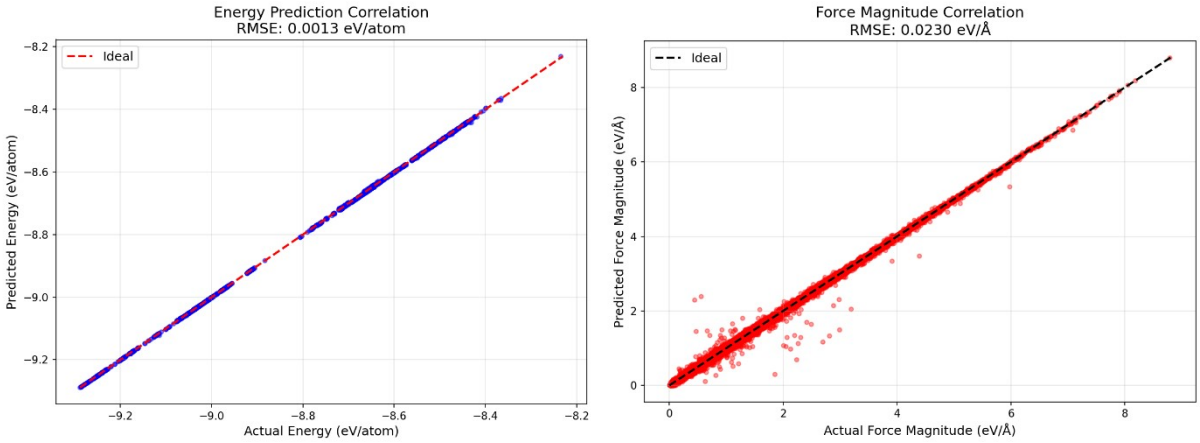


Figure S2. RMSE of energies and force magnitudes for DPA-3.1 potential

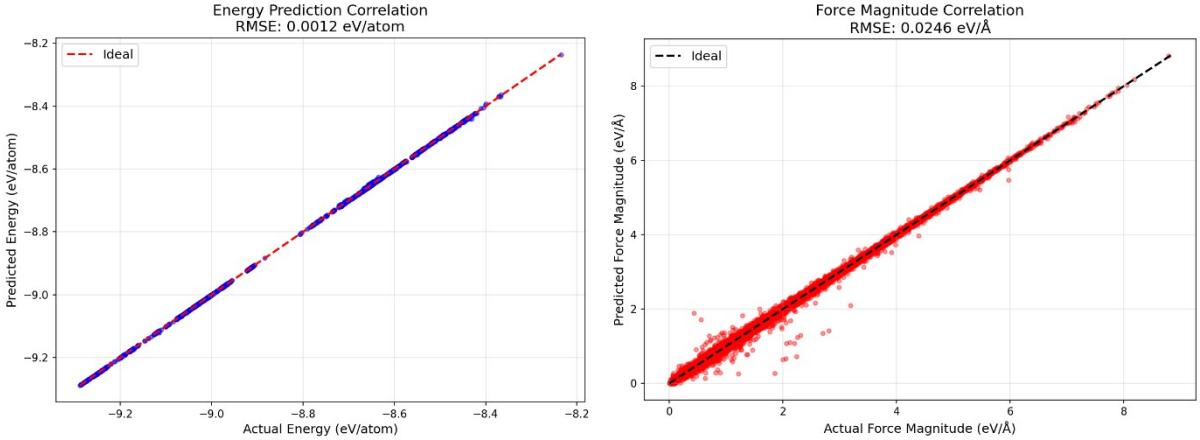


Figure S3. RMSE of energies and force magnitudes for DPA-2.4-fine potential

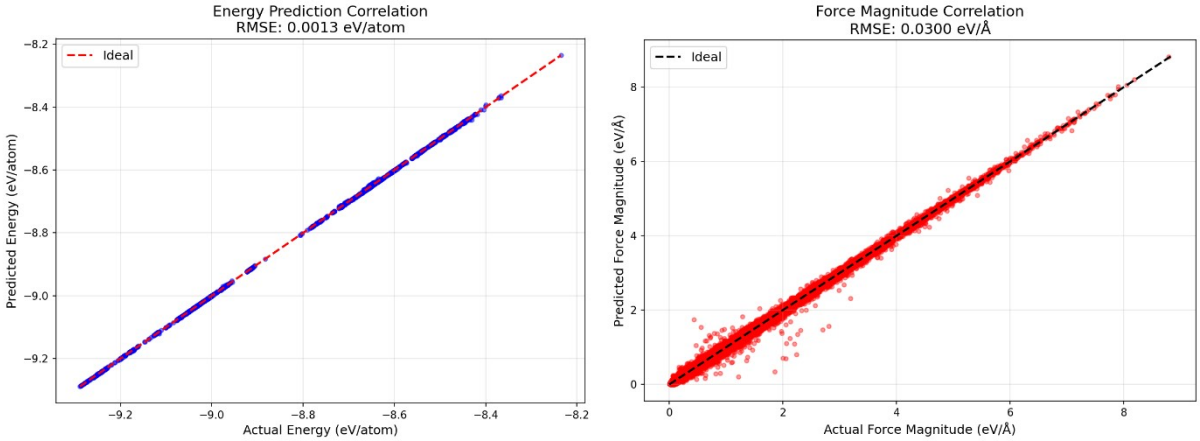


Figure S4. RMSE of energies and force magnitudes for DPA-2.4 potential

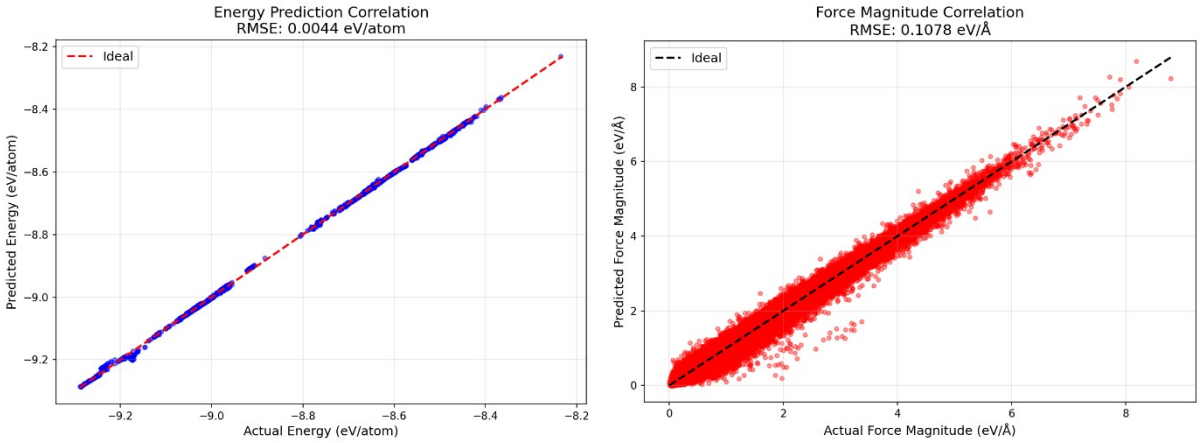


Figure S5. RMSE of energies and force magnitudes for DP-e2 potential

**Additional validation results and dataset sensitivity**

To evaluate the sensitivity of the potential to the composition of the training dataset, additional models were trained with selected subsets of structures excluded from the database. In particular, two modified datasets were considered: (i) without all iridagraphene-related structures and (ii) without iridagraphene structures lacking adsorbed Li atoms. The resulting fine-tuned potentials are denoted as DPA-3-fine-2 and DPA-3-fine-3, respectively.

Tables S3 and S4 summarize the RMSE values for energies and force magnitudes obtained for different DeePMD models and system classes. In addition to the original models discussed in the main text, these tables also include the modified DPA-3-fine-2 and DPA-3-fine-3 potentials trained using reduced datasets.

**Table S3**. RMSE of energies (meV/atom) for each model and each trained interatomic potential

| model | DPA-2-fine | DPA-2 | DPA-3-fine | DPA-3-fine-2 | DPA-3-fine-3 | DPA-3 | DP-e2 |
|---|---|---|---|---|---|---|---|
| graphene | 0.4 | 0.6 | 0.8 | 2.2 | 0.5 | 0.2 | 0.4 |
| graphene_vac | 1.0 | 1.6 | 1.3 | 0.7 | 0.6 | 0.4 | 26.1 |
| graphene_dvac | 0.4 | 0.2 | 1.0 | 5.5 | 0.4 | 0.3 | 11.4 |
| graphite | 0.6 | 0.8 | 1.4 | 1.2 | 0.8 | 0.4 | 1.6 |
| SWNT(5, 5) | 0.1 | 0.4 | 0.6 | 0.5 | 0.5 | 0.3 | 2.5 |
| SWNT(8, 0) | 0.1 | 0.2 | 0.6 | 0.4 | 0.4 | 0.3 | 2.1 |
| biphenilen | 0.8 | 0.2 | 0.7 | 0.4 | 0.5 | 1.7 | 6.8 |
| psi-graphene | 0.4 | 0.7 | 0.5 | 1.4 | 0.2 | 0.6 | 0.9 |
| irida-graphene | 0.6 | 0.5 | 1.0 | 107.5 | 1.7 | 2.3 | 4.4 |
| tpdh-graphene | 0.4 | 0.5 | 1.2 | 0.5 | 0.3 | 1.6 | 2.6 |
| N-graphene | 0.2 | 0.6 | 0.8 | 1.6 | 0.6 | 0.2 | 14.7 |
| N-pyridinic | 0.5 | 0.5 | 1.0 | 1.9 | 0.6 | 0.5 | 12.4 |
| C2N | 1.1 | 1.2 | 2.0 | 1.9 | 0.2 | 2.1 | 1.5 |
| C2N_3D | 3.3 | 2.9 | 2.5 | 6.1 | 4.2 | 2.5 | 3.1 |

| | | | | | | | |
|---|---|---|---|---|---|---|---|
| C2N+3Li | 0.9 | 1.0 | 1.0 | 1.8 | 0.7 | 1.0 | 1.4 |
| C2N_3D+3Li | 0.0 | 0.2 | 0.7 | 1.3 | 0.1 | 0.4 | 0.2 |
| graphene+1Li | 1.3 | 1.4 | 1.4 | 2.2 | 1.4 | 1.2 | 1.4 |
| graphene+3Li | 1.0 | 1.8 | 0.4 | 2.5 | 0.6 | 0.5 | 4.8 |
| graphite+3Li | 0.6 | 0.6 | 0.9 | 2.2 | 0.6 | 0.7 | 1.4 |
| biphenilen+3Li | 0.8 | 0.7 | 0.8 | 0.8 | 0.7 | 1.2 | 4.1 |
| psi-graphene+3Li | 0.4 | 0.5 | 0.2 | 2.9 | 0.1 | 0.2 | 7.9 |
| irida-graphene+3Li | 0.4 | 0.4 | 0.3 | 126.4 | 11.8 | 0.8 | 2.3 |
| tpdh-graphene+4Li | 0.7 | 0.8 | 1.0 | 1.4 | 0.7 | 1.1 | 2.4 |
| SWNT(5, 5)+1Li | 0.2 | 0.6 | 0.4 | 1.3 | 0.4 | 0.2 | 2.8 |
| SWNT(5, 5)+5Li | 0.7 | 0.9 | 0.7 | 0.7 | 0.6 | 0.8 | 1.3 |
| SWNT(5, 5)+10Li | 1.6 | 1.9 | 1.1 | 1.6 | 1.0 | 1.0 | 3.4 |
| SWNT(8, 0)+5Li | 0.4 | 0.7 | 0.3 | 0.4 | 0.1 | 0.3 | 4.5 |
| SWNT(8, 0)+10Li | 1.4 | 1.8 | 0.6 | 0.8 | 0.8 | 0.5 | 6.0 |
| TOC | 0.9 | 1.2 | 0.7 | 0.4 | 0.2 | 0.8 | 1.4 |
| TOC_3D | 5.1 | 4.5 | 3.6 | 4.4 | 3.9 | 3.5 | 4.1 |
| TOC+3Li | 1.3 | 1.4 | 1.4 | 1.6 | 1.3 | 1.4 | 1.8 |
| TOC_3D+3Li | 1.4 | 1.3 | 1.9 | 2.1 | 1.7 | 2.1 | 1.7 |
| Total | 1.2 | 1.3 | 1.3 | 26.2 | 2.4 | 1.3 | 4.4 |

**Table S4**. RMSE of force magnitudes (meV/Å) for each model and each trained interatomic potential

| model | DPA-2-fine | DPA-2 | DPA-3-fine | DPA-3-fine-2 | DPA-3-fine-3 | DPA-3 | DP-e2 |
|---|---|---|---|---|---|---|---|
| graphene | 13.25 | 20.75 | 8.36 | 19.98 | 8.56 | 10.23 | 86.25 |
| graphene_vac | 71.88 | 77.81 | 59 | 74.84 | 57.66 | 60.54 | 149.33 |
| graphene_dvac | 22.15 | 27.05 | 12.06 | 30.52 | 11.25 | 12.91 | 243.13 |
| graphite | 11.1 | 18.67 | 10.04 | 21.24 | 10.3 | 14.58 | 72.31 |
| SWNT(5, 5) | 14.32 | 17.33 | 13.41 | 20.46 | 12.95 | 14.41 | 100.15 |
| SWNT(8, 0) | 11.14 | 15.19 | 10.5 | 19.36 | 9.51 | 11.1 | 111.88 |
| biphenilen | 31.52 | 43.83 | 20.48 | 47.91 | 20.8 | 27.66 | 170.13 |
| psi-graphene | 22.61 | 33.25 | 15.34 | 33.31 | 16.37 | 19.56 | 134 |
| irida-graphene | 25.2 | 34.9 | 19.09 | 480.69 | 22.33 | 23.44 | 131.61 |
| tpdh-graphene | 29.27 | 42.14 | 20.43 | 43.36 | 19.21 | 27.41 | 142.76 |
| N-graphene | 7.44 | 9.38 | 5.03 | 13.77 | 5.12 | 5.67 | 73.83 |
| N-pyridinic | 58.59 | 57.92 | 54.98 | 59.56 | 60.37 | 62.41 | 152.36 |
| C2N | 21.11 | 29.79 | 11.41 | 24.04 | 12.19 | 13.03 | 104.4 |
| C2N_3D | 11.05 | 15.22 | 11.67 | 17.85 | 12.03 | 10.1 | 66.06 |
| C2N+3Li | 18.02 | 23.78 | 12.19 | 20.39 | 12.38 | 13.25 | 70.76 |
| C2N_3D+3Li | 17.95 | 22.54 | 10.88 | 28.8 | 11.81 | 12.56 | 114.42 |

| | | | | | | | |
|---|---|---|---|---|---|---|---|
| graphene+1Li | 16.89 | 25.59 | 11.18 | 24.27 | 11.62 | 13.72 | 86.1 |
| graphene+3Li | 22 | 30.25 | 16.22 | 31.84 | 16.21 | 18.09 | 93.18 |
| graphite+3Li | 13 | 19.3 | 10.83 | 21.7 | 10.98 | 13.21 | 61.74 |
| biphenilen+3Li | 21.58 | 27.93 | 15.85 | 29.48 | 16.09 | 18.98 | 104.85 |
| psi-graphene+3Li | 15.36 | 21.48 | 11.56 | 21.66 | 11.41 | 13.06 | 95.58 |
| irida-graphene+3Li | 20.44 | 26.53 | 14.51 | 495.39 | 150.09 | 18.14 | 101.9 |
| tpdh-graphene+4Li | 36.67 | 50.47 | 26.19 | 48.95 | 26.26 | 34.11 | 148.77 |
| SWNT(5, 5)+1Li | 14.7 | 21.01 | 12.92 | 23.21 | 12.41 | 13.83 | 104.14 |
| SWNT(5, 5)+5Li | 33.53 | 41.04 | 25.82 | 44.09 | 25.78 | 29.28 | 122.72 |
| SWNT(5, 5)+10Li | 54.35 | 61.5 | 42.56 | 64.6 | 43.17 | 45.36 | 150.14 |
| SWNT(8, 0)+5Li | 43.93 | 51.58 | 31.47 | 49.23 | 34.64 | 33.44 | 231.3 |
| SWNT(8, 0)+10Li | 66.3 | 76.48 | 44.4 | 72.08 | 40.08 | 45.38 | 214.81 |
| TOC | 14.46 | 23.29 | 10.08 | 22.45 | 10.04 | 13.4 | 80.89 |
| TOC_3D | 10.84 | 15.13 | 12.4 | 19.39 | 12.45 | 14.56 | 68.62 |
| TOC+3Li | 15.95 | 19.72 | 12.05 | 20.33 | 11.95 | 13.71 | 61.98 |
| TOC_3D+3Li | 23.32 | 32.31 | 18.16 | 37.18 | 18.11 | 24.75 | 117.03 |
| Total | 24.62 | 29.99 | 19.86 | 122.88 | 39.05 | 23.01 | 107.82 |

Table S5 compares Li adsorption energies predicted by these models against VASP reference data for different classes of carbon-based materials. In the adsorption-site labels, the first number denotes the ring size. For heteroatom-containing rings, the number and type of non-carbon atoms are additionally indicated.

The results show that excluding even relatively small subsets of structurally related configurations may noticeably deteriorate prediction accuracy across multiple material families. This behavior indicates that the model learns transferable structural and chemical relationships shared among different systems rather than merely memorizing local adsorption environments.

**Table S5**. Li adsorption energies $E_{ads}$ (eV) predicted by different DeePMD potentials trained with modified datasets, compared with VASP reference values

| Adsorption center | VASP $E_{ads}$ | DP-3.1-fine | | DP-3.1-3M | | DP-3.1-fine-2 | | DP-3.1-fine-3 | |
|---|---|---|---|---|---|---|---|---|---|
| | | $E_{ads}$ | % | $E_{ads}$ | % | | | $E_{ads}$ | % |
| Biphenilen-4 | -1.872 | -1.879 | 0.4 | -1.535 | 18.0 | -1.848 | 1.3 | -2.104 | 12.4 |
| Biphenilen-6 | -1.926 | -1.964 | 2.0 | -1.648 | 14.4 | -1.918 | 0.4 | -2.135 | 10.9 |
| Biphenilen-8 | -1.844 | -1.892 | 2.6 | -1.568 | 15.0 | -1.878 | 1.8 | -2.050 | 11.1 |
| Graphene-6 | -1.366 | -1.292 | 5.5 | -1.740 | 27.4 | -1.300 | 4.9 | -1.331 | 2.6 |
| Irida-3 | -1.751 | -1.774 | 1.3 | -1.682 | 3.9 | -1.320 | 24.6 | -1.536 | 12.3 |
| Irida-6 | -2.025 | -2.085 | 3.0 | -1.882 | 7.0 | -1.656 | 18.2 | -1.689 | 16.6 |
| Irida-8 | -2.016 | -2.065 | 2.4 | -1.923 | 4.6 | -1.672 | 17.1 | -1.653 | 18.0 |
| Psigraphene-5 | -2.311 | -2.623 | 13.5 | -1.793 | 22.4 | -2.362 | 2.2 | -2.807 | 21.5 |
| Psigraphene-6 | -2.276 | -2.595 | 14.0 | -1.734 | 23.8 | -2.358 | 3.6 | -2.718 | 19.4 |
| Psigraphene-7 | -2.315 | -2.658 | 14.8 | -1.756 | 24.1 | -2.398 | 3.6 | -2.768 | 19.6 |
| SWNT(5,5)-6 | -1.498 | -1.417 | 5.4 | -1.764 | 17.8 | -1.330 | 11.2 | -1.452 | 3.1 |
| Tpdh-4 | -2.247 | -2.305 | 2.6 | -1.919 | 14.6 | -2.204 | 1.9 | -2.408 | 7.2 |
| Tpdh-5 | -2.298 | -2.352 | 2.4 | -2.075 | 9.7 | -2.248 | 2.2 | -2.455 | 6.8 |
| Tpdh-6 | -2.270 | -2.336 | 2.9 | -2.055 | 9.5 | -2.220 | 2.2 | -2.435 | 7.2 |
| Tpdh-10 | -2.324 | -2.454 | 5.6 | -2.095 | 9.9 | -2.259 | 2.8 | -2.537 | 9.1 |
| C2N-6-2N | -1.606 | -1.616 | 0.6 | -1.742 | 8.5 | -1.622 | 1.0 | -1.720 | 7.0 |
| C2N-6 | -1.396 | -1.406 | 0.7 | -1.730 | 24.0 | -1.415 | 1.4 | -1.516 | 8.6 |
| C2N-18-4N | -4.504 | -4.555 | 1.1 | -4.087 | 9.3 | -4.683 | 4.0 | -4.603 | 2.2 |
| TOC-5-1O | -1.024 | -0.950 | 7.2 | -1.220 | 19.1 | -0.732 | 28.5 | -1.043 | 1.9 |
| TOC-6 | -1.185 | -1.110 | 6.3 | -1.501 | 26.7 | -0.940 | 20.6 | -1.174 | 0.9 |
| TOC-8 | -1.102 | -1.007 | 8.7 | -1.436 | 30.3 | -0.907 | 17.7 | -1.073 | 2.7 |

| | | | | | | | | | |
|---|---|---|---|---|---|---|---|---|---|
| TOC-16-4O | -2.839 | -2.803 | 1.3 | -2.812 | 1.0 | -2.596 | 8.6 | -2.792 | 1.7 |
| C60-5 | -1.602 | -0.190 | 88.1 | -2.329 | 45.4 | -4.872 | 204.0 | -1.735 | 8.3 |
| C60-6 | -1.599 | -0.203 | 87.3 | -2.684 | 67.9 | -4.999 | 212.6 | -1.619 | 1.2 |
| SWNT(6,2)-6 | -1.558 | -1.324 | 15.0 | -1.862 | 19.5 | -1.771 | 13.7 | -1.432 | 8.1 |
| SWNT(7,3)-6 | -1.519 | -1.494 | 1.7 | -1.765 | 16.1 | -1.302 | 14.3 | -1.550 | 2.0 |
| SWNT(7,7)-6 | -1.520 | -1.546 | 1.7 | -1.766 | 16.2 | -1.375 | 9.6 | -1.578 | 3.8 |
| SWNT(8,8)-6 | -1.521 | -1.518 | 0.2 | -1.768 | 16.2 | -1.375 | 9.6 | -1.532 | 0.7 |
| SWNT(9,0)-6 | -1.543 | -1.534 | 0.6 | -1.790 | 16.1 | -1.356 | 12.1 | -1.617 | 4.8 |
| SWNT(10,0)-6 | -1.345 | -1.575 | 17.1 | -1.795 | 33.5 | -1.322 | 1.7 | -1.652 | 22.8 |

Table S6 presents the wall-time per molecular dynamics step for tetraoxa[8]circulene calculated using different interatomic potentials on an NVIDIA Tesla V100 (16 GB) GPU. Table S7 summarizes the RMSD values between equilibrium ab initio structures and geometries optimized using the DPA-3-fine potential for various two-dimensional materials and carbon nanotubes.

**Table S6**. Wall-time per molecular dynamics step (ms) for tetraoxa[8]circulene using different interatomic potentials on an NVIDIA Tesla V100 (16 GB) GPU

| Number of atoms | e2_compr | e2 | DPA2-compr | DPA2 | DPA3 |
|---|---|---|---|---|---|
| 99 | 0.0091 | 0.0182 | 0.026 | 0.0269 | 0.0559 |
| 396 | 0.0117 | 0.0357 | 0.0672 | 0.0687 | 0.1356 |
| 792 | 0.0162 | 0.0591 | 0.117 | 0.12 | 0.2362 |
| 1188 | 0.0209 | 0.0827 | 0.1646 | 0.1689 | |
| 1584 | 0.0251 | 0.1057 | 0.2153 | 0.2211 | |
| 1782 | 0.0276 | 0.1176 | 0.2377 | 0.2452 | |
| 1980 | 0.0295 | 0.1282 | 0.2611 | 0.2684 | |
| 3168 | 0.0438 | 0.1991 | | | |
| 4752 | 0.0622 | | | | |
| 6336 | 0.08 | | | | |
| 8019 | 0.101 | | | | |
| 9900 | 0.1208 | | | | |
| 14256 | 0.1711 | | | | |
| 16731 | 0.2045 | | | | |
| 18810 | 0.2289 | | | | |

**Table S7**. RMSD between equilibrium ab initio structures and geometries obtained using the DPA-3-fine potential for various two-dimensional systems and carbon nanotubes

| Model | RMSD, pm |
|---|---|
| TPDH+1Li | 0.0063, 0.2947, 0.0016, 0.0163 |
| TOC | 0.0003 |
| TOC+1Li | 0.0287, 0.3652, 0.0049, 0.0066 |

| | |
|---|---|
| C2N | 0.0002 |
| C2N+1Li | 0.2038, 0.3594, 0.0426 |
| SWNT(5, 5) | 0.0001 |
| SWNT(5, 5)+1Li | 0.0355 |
| SWNT(6, 2) | 0.0007 |
| SWNT(6, 2)+1Li | 0.0255 |
| SWNT(7, 3) | 0.0004 |
| SWNT(7, 3)+1Li | 0.0266 |
| SWNT(7, 7) | 0.0004 |
| SWNT(7, 7)+1Li | 0.0352 |
| SWNT(8, 8) | 0.0004 |
| SWNT(8, 8)+1Li | 0.0279 |
| SWNT(9, 0) | 0.0004 |
| SWNT(9, 0)+1Li | 0.0228 |
| SWNT(10, 0) | 0.0009 |
| SWNT(10, 0)+1Li | 0.0179 |

**Methodological details of elastic properties determination**

The elastic properties of two-dimensional materials and carbon nanotubes were evaluated in the vicinity of the equilibrium configuration using total energy calculations under small uniaxial deformations. All deformations were kept within the linear elastic regime, with strain amplitudes not exceeding a few percent, ensuring a quadratic dependence of the total energy on strain.

For each system, a series of strained configurations was generated by applying longitudinal strain ε to the simulation cell. For two-dimensional materials, the strain was applied in-plane, while for carbon nanotubes it was applied along the tube axis. For each imposed longitudinal strain, the transverse strain component was determined by minimizing the total energy, allowing extraction of the Poisson's ratio.

At each strain value, atomic positions were fully relaxed while keeping the deformed cell parameters fixed. Total energies were calculated both using density functional theory (DFT) and the DPA-3-fine machine-learned potential, ensuring a consistent comparison between the two approaches.

Near equilibrium, the total energy as a function of strain was fitted by a quadratic expression

$$E(\varepsilon) = E_0 + C\varepsilon^2,$$

where $E_0$ is the energy of the undeformed system and $C$ is the curvature coefficient. Elastic moduli were obtained by normalizing the coefficient $C$ with respect to the effective geometry of the system.

For two-dimensional materials, the two-dimensional Young's modulus was defined as

$$E^{2D} = \frac{2C}{A_0},$$

where $A_0$ is the equilibrium in-plane area of the simulation cell. When comparison with literature data expressed in three-dimensional units (GPa) was required, an effective layer thickness was introduced. For graphene and related materials, this thickness was taken to be equal to the interlayer spacing in the corresponding bulk material.

For carbon nanotubes, the Young's modulus was calculated by normalizing the curvature coefficient with respect to the effective nanotube volume $V_0 = \pi dtL$,

where $d$ is the nanotube diameter, $L$ is the length of the simulation cell, and $t$=0.34 nm is the effective wall thickness, corresponding to the interlayer spacing in graphite. This definition is consistent with common experimental and theoretical approaches used to determine the elastic moduli of carbon nanotubes [1].

The Poisson's ratio was extracted from the linear relation between transverse and longitudinal strains in the small-deformation limit. All reported elastic constants correspond to zero-temperature values obtained from static total energy calculations.

**Methodological details of diffusion barrier determination**

To evaluate the diffusion barrier of a lithium atom between neighboring adsorption sites, a series of single-point calculations was performed. The lithium atom was systematically displaced along a straight path connecting the equilibrium positions corresponding to adjacent adsorption sites, while the positions of all other atoms were kept fixed. The calculations were carried out using both VASP and the trained DeePMD potential (DP-3.1-fine). Figures S6–S8 show the atomic structures with indicated adsorption sites for biphenylene, $C_2N$, and TOC, respectively, along with the corresponding energy profiles for lithium migration between these sites.

For most migration pathways, the DeePMD potential reproduces the DFT energy profiles with good quantitative agreement in the physically relevant energy range corresponding to realistic diffusion barriers. An exception was observed for the TOC 1–2 migration path, where the Li atom approaches an oxygen atom at very short distances. In this case, the DeePMD and DFT energy profiles qualitatively diverge at highly unfavorable configurations corresponding to very large energies (up to ~15 eV in the DFT calculations). However, the agreement remains reasonable up to energies of approximately 1.5–2 eV, which are significantly above the thermally accessible diffusion barriers relevant for practical Li migration processes.

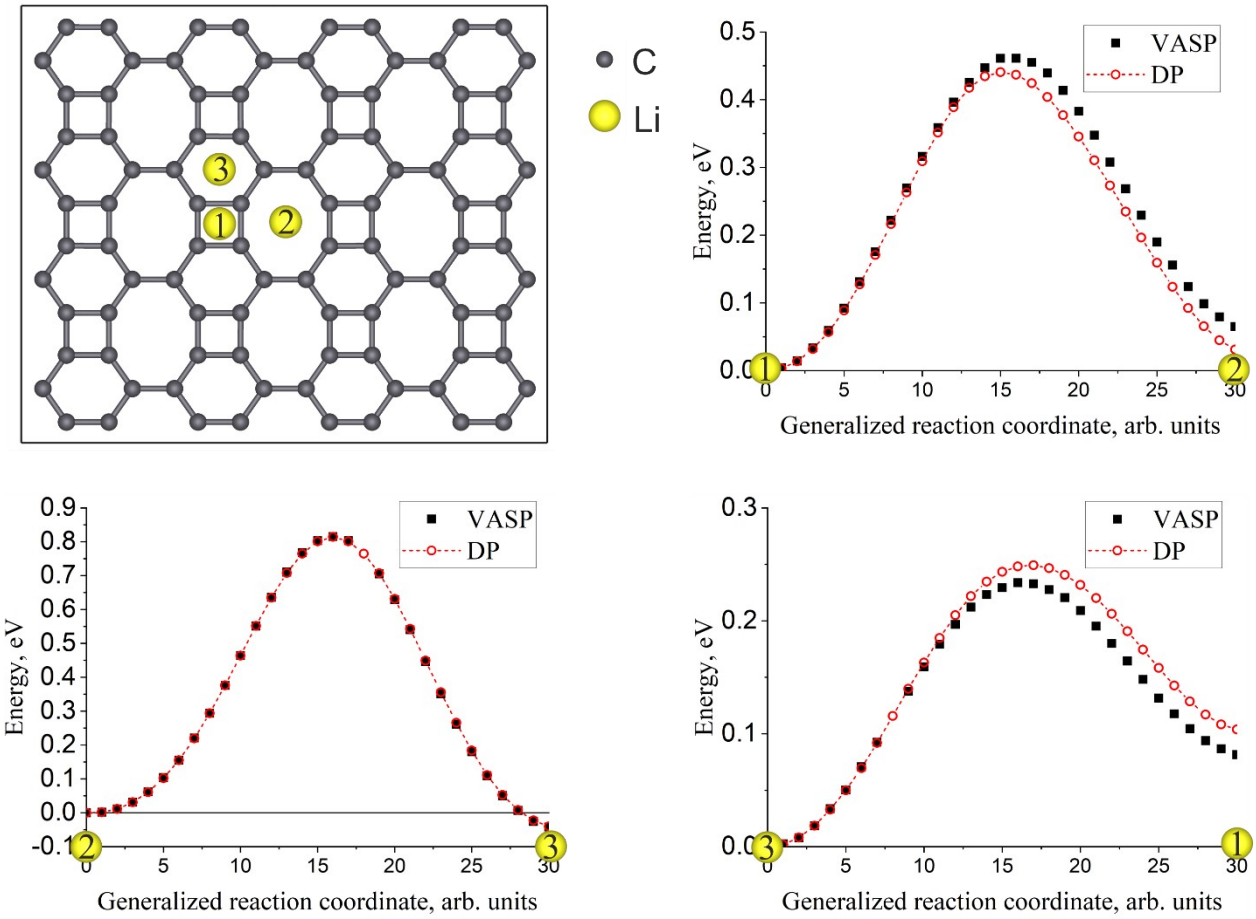


Figure S6. Energy profile for Li atom migration along a linear path between two adsorption sites in biphenylene. Results obtained using VASP and DeePMD are shown for comparison.

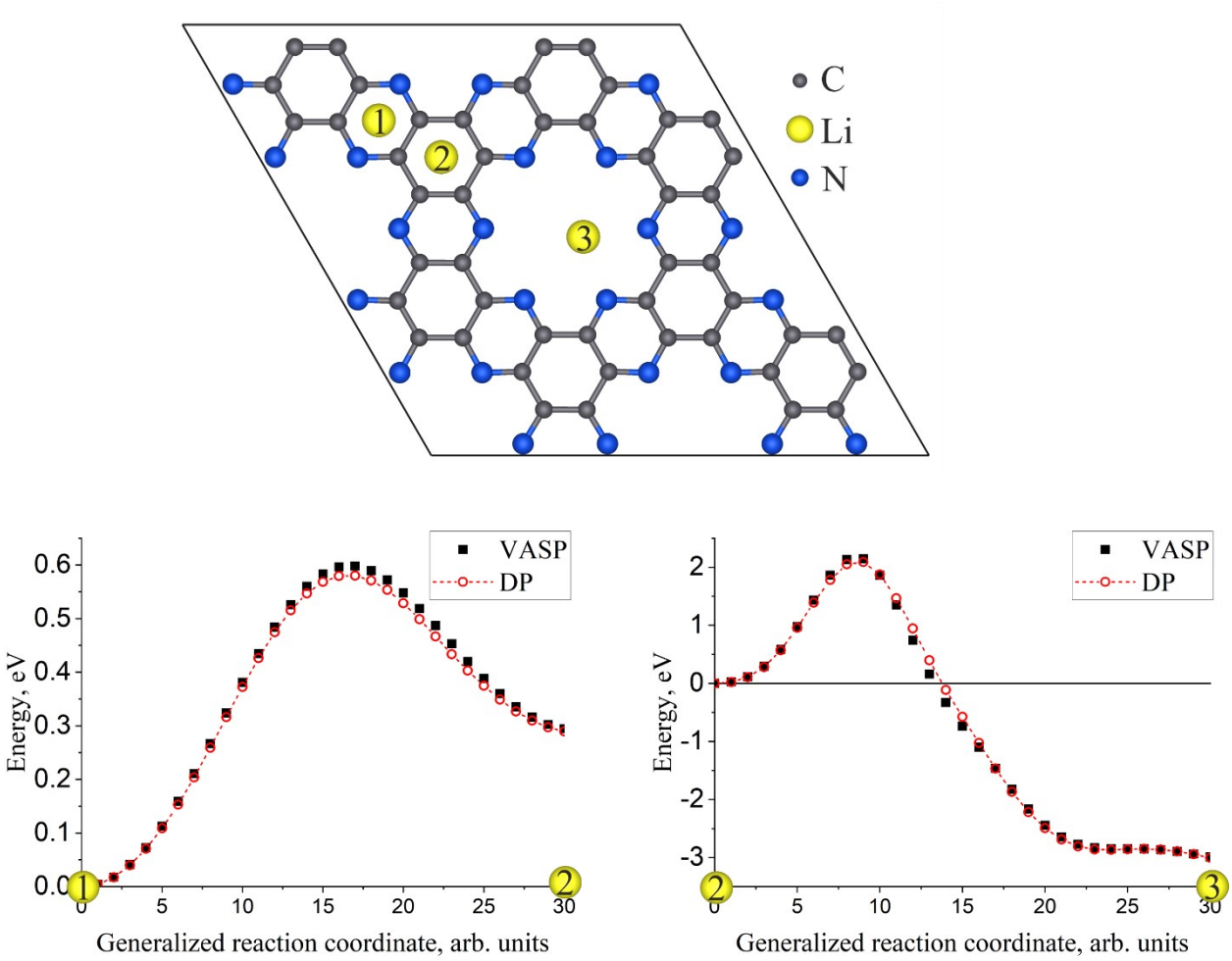


Figure S7. Energy profile for Li atom migration along a linear path between two adsorption sites in C2N. Results obtained using VASP and DeePMD are shown for comparison.

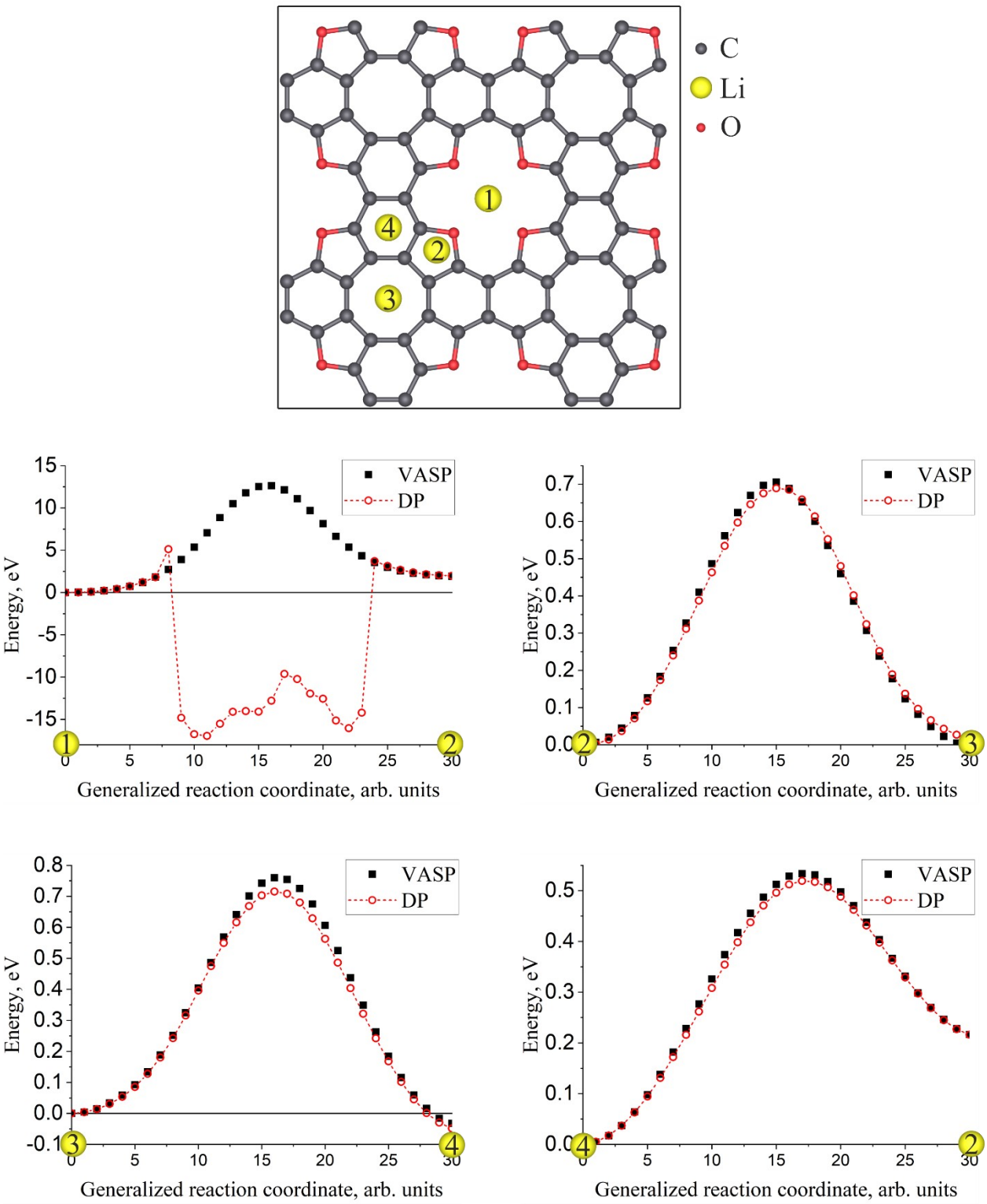


Figure S8. Energy profile for Li atom migration along a linear path between two adsorption sites in TOC. Results obtained using VASP and DeePMD are shown for comparison.

1. Wu Y. и др. Determination of the Young's Modulus of Structurally Defined Carbon Nanotubes // Nano Lett. 2008. Т. 8, № 12. С. 4158–4161.